



This is a repository copy of *Failure analysis of pipeline indents using steel precision balls under subsea conditions*.

White Rose Research Online URL for this paper:
<http://eprints.whiterose.ac.uk/118321/>

Version: Accepted Version

Article:

Gill, W.S., Marshall, M.B., Lewis, R. et al. (2 more authors) (2018) Failure analysis of pipeline indents using steel precision balls under subsea conditions. *Tribology International*, 118. pp. 524-537. ISSN 0301-679X

<https://doi.org/10.1016/j.triboint.2017.06.007>

Article available under the terms of the CC-BY-NC-ND licence
(<https://creativecommons.org/licenses/by-nc-nd/4.0/>).

Reuse

This article is distributed under the terms of the Creative Commons Attribution-NonCommercial-NoDerivs (CC BY-NC-ND) licence. This licence only allows you to download this work and share it with others as long as you credit the authors, but you can't change the article in any way or use it commercially. More information and the full terms of the licence here: <https://creativecommons.org/licenses/>

Takedown

If you consider content in White Rose Research Online to be in breach of UK law, please notify us by emailing eprints@whiterose.ac.uk including the URL of the record and the reason for the withdrawal request.



eprints@whiterose.ac.uk
<https://eprints.whiterose.ac.uk/>

Failure analysis of pipeline indents using steel precision balls under subsea conditions

W. S. Gill^{a, b, *}, M. B. Marshall^a, R. Lewis^a, B. Hall^b, S. Bolton^b

^aThe University of Sheffield, Department of Mechanical Engineering, Mappin Street, Sheffield, UK.

^bHydratight UK Ltd., Access 10, Bentley Road South, Walsall, UK.

Abstract

Mechanical connectors used to repair sub-sea pipe lines can use balls to achieve grip on the pipe surface. While designed to indent the pipe surface, it has been found that some balls skid instead which reduces the connection integrity.

This work was aimed at finding important features which relate to rolling and skidding of precision balls on the surface of pipes. A skidded ball is associated with a failure and a rolled ball is associated with success. Experiments simulating the activation were performed and compared with analytical models. Several features such as friction, ball size, material hardness and surface finish were identified as important for understanding the transition of the ball from roll into skid. The results of the surface and subsurface analysis correlated well with the model output. Once the important features are verified, progress can be made to achieve production of more robust connectors (from successful activations) leading to better customer confidence in buying mechanical pipeline connector products.

Keywords: contact mechanics, friction, fatigue, microstructure, structural collapse, subsea, and traction.

*Waljinder Singh Gill (waljinder.gill@hydratight.com).

1. INTRODUCTION

Sub-sea pipe-lines may require mechanical connectors as part of a repair strategy. In such connectors, a series of precision balls arranged circumferentially around the pipe in axial rows are used to achieve a mechanical grip (Figure 1a). As the connector is actuated the balls roll along a taper housing (Figure 1b), leading to an increasing radial force. The taper housing angle is kept at 10 degrees with the respect to the x-axis in the Figure. This radial force causes the ball to indent the pipe material, leaving a teardrop (Figure 1c) shaped impression, and results in the connector gripping the pipe [4]. The scale of the teardrop (0.5mm indent depth) in Figure 1c is proportional to the size of the precision ball used (\varnothing 30mm). Unfortunately the teardrop formation does not always happen, and in some instances it has been noted that the balls skid

instead of rolling along the taper and indenting, resulting in the connector not gripping the pipe. In this case, a witness mark is evident on the pipe surface, though no actual deformation or radial load increase occurs.

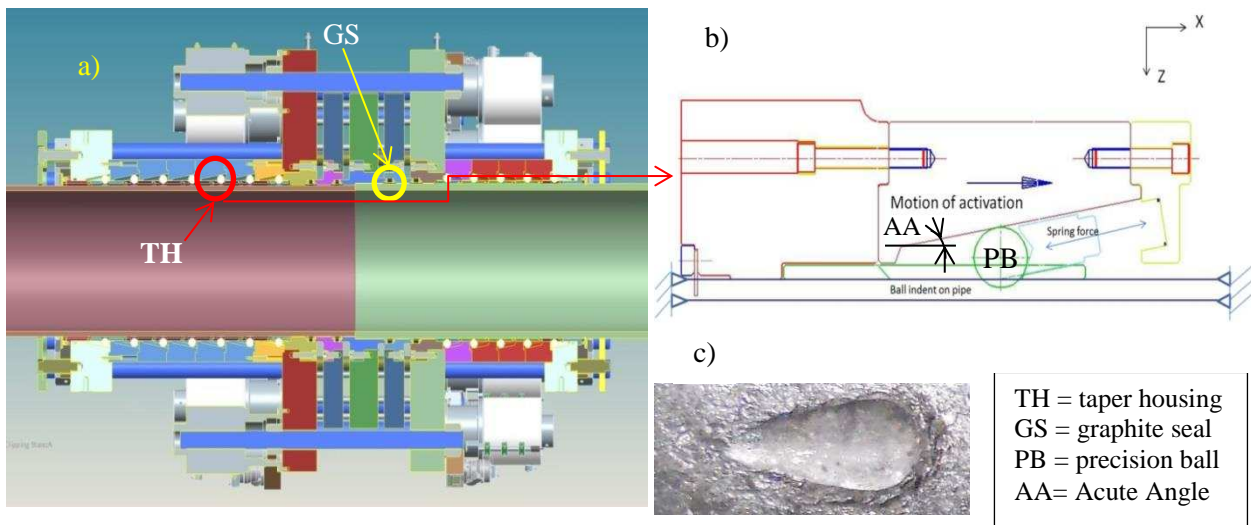


Figure 1: a) Illustration of a typical mechanical connector. b) Ball activation mechanism; Angle = $\pi/18$ rad. c) A typical teardrop formation on a pipe wall after indentation.

Previous investigations by Hydratight have linked the probability of a skid to factors such as the taper angle (>11 degrees), along with pipe tolerance and surface finish [1].

In this study, the contact conditions occurring between the ball and pipe material have been simulated using a Bruker® UMT 3 Tribometer, with the aim of investigating the factors that lead to the ball either rolling and indenting, or skidding. This approach has been coupled with analytical modelling of the contact conditions present, in order to assess the likely impact of factors such as the mechanical properties of the materials, surface roughness and friction coefficient. The outcomes of this study will then be used by Hydratight to identify conditions when skidding is likely, helping make failure predictions more robust.

Similar work (related to ball indent analysis) was reviewed for background research purposes. Kaneta et al modelled the surface roughness by engineering a constant height and wavelength bumps on smooth steel surface[20]. Bhushan proposed a 3-D model which could produce a surface of varying size and height asperity distributions, which would replicate a real surface. The asperities were noticed to be elastically and elastic-plastically deforming by an elastic sphere in motion depending on the contact mechanics and the asperity shape and orientations[22]. The chrome steel has a high hardness value and is almost 3-4 times harder than the pipe surface. This is equivalent of using a rigid sphere in motion over a model replicating a real surface. In the initialization process, the ball would deform the asperities elastically but would eventually plastically deform all asperities in contact.

A FEA model using frictional contact was presented by Kogut wherein the deformations were in the elastic-plastic region. The two rough surfaces in contact were tested in a sliding motion [21]. The friction was found to be affected by the amount of permanent deformation and adhesion between the two surfaces. The adhesion between the chrome steel precision ball and carbon steel material is negligible.

Bogy et al found, using a point contact microscope, that the hardness of a material increases with small indent depth and loads but the hardness becomes insensitive once a limit has reached [23]. The indent depths discussed in this paper are higher than the range tested by Bogy (50-100nm). This means the hardness value would not change much for the higher range of indents but will change during the indent initialization process.

A UMT 3 tribometer with slow reciprocating module was used to analyse the rolling friction of balls rolling friction dependence on rotational speed in dry contacts [2]. The results were then compared to an analytical model which showed high correlation with the experimental results. The analytical model predicted the values and location of the maximum shear stress based on the mechanical properties of the materials in contact and friction/traction coefficients. If the location of the maximum shear stress is away from the centre of the ball and close to the surface, it means the ball is sliding opposed to rolling when the maximum shear stress is located subsurface towards the centre of the ball.

There were also comparisons done on the rolling friction of balls on micro and macro levels in dry and lubricated or wet conditions for which the results fitted well with the analytical models [3].

The main objective of the work outlined in this paper was to understand the complex contact mechanics between the balls and the pipe and identify the key parameters that cause the balls to skid from rolling conditions. This information can be used to ensure better integrity of the connector and eventually of the pipeline system.

To our knowledge, Hertzian contact models have been rarely compared against experiments using precision balls in sliding and rolling motion. The key novel aspect of this paper is the validation of the analytical theory for this scenario allowing improved confidence in using the model for the ball 'skidding' problem.

2. CONNECTOR BALL-PIPE CONTACT MECHANICS ANALYSIS

2.1. Activation of mechanical connector

Activation is the process of closing the connector to effect a pressure seal and create a firm grip onto the concerning pipe. During the process, precision balls are used to indent onto the pipe surface while they roll using a taper housing which traverses axially, as illustrated in Figure 1b. The ball rolls in the direction of the activation and progress to move to the lower part of the inclined surface (10 degrees) under generation of radial force from the taper geometry. The spring is to ensure all balls are in contact with the pipe considering

that gravity will affect some of the balls. Once the ball has touched the pipe and the ball starts rolling, the spring-force is no longer required. The activation process was modelled using an analytical approach which was compared with the results from physical testing. The comparison will give a sense of how well the model actually operates in terms of accuracy.

2.2. Mechanics

In order to find which features of the ball indent mechanism lead to ball skidding, a full mechanical assessment of the ball indentation process was carried out. The forces acting on the ball while it is forced to indent into the pipe material can be divided into vertical (F_v) and horizontal forces (F_h) respectively as shown in Figure 2. These forces on the ball are resisted by the reactions at the contact and due to friction arising from the rolling or skidding motion. If the ball is rolling (due to rolling force F_{roll} in Figure 2), there is a frictional force opposing this motion defined as $F_{\mu roll}$. On the other hand, if the ball is sliding, the force of sliding F_{skid} is opposed by F_{tan} .

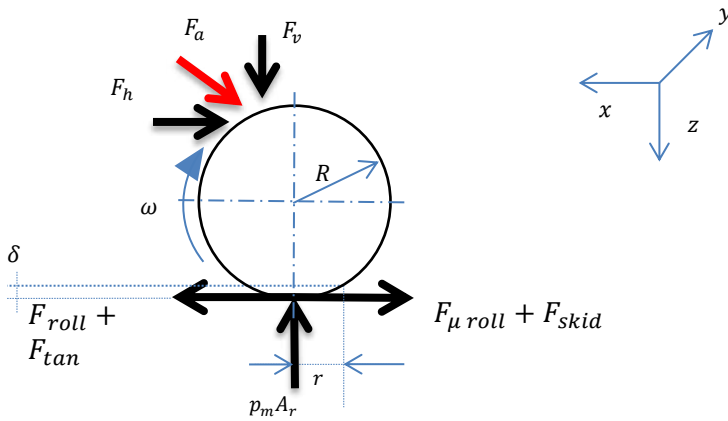


Figure 2: Illustration of the ball indent mechanics involving forces leading to roll/skid.

Note that the F_{tan} and F_{roll} are different in the sense that one is due to sliding and the other is helping the rolling motion respectively. The sliding resistance is always higher than the 'elastic' rolling friction. As the ball starts rolling down the taper, it has to indent the pipe material with an indent radius r . The indent radius keeps changing with the amount of indent depth, δ . Since the ball is spherical and the outer surface of the pipe is cylindrical, the contact type is a standard Hertzian point contact [5, 8, 12, 16].

For precision balls (1.25% Chrome EN31 [Gr 5-100] for low carbon steel pipes or stainless steel AISI420 for stainless steel and duplex connectors), the Elastic modulus values are normally taken as $E = 213$ GPa and ν as 0.3 for contact mechanics of chrome steel balls. Usually, the indenting material is steel and has an elastic modulus of 185-215 GPa and ν of 0.25 - 0.35. The Hertzian area in Figure 2, $A_r = \pi r^2$, where r is the Hertzian contact radius and contact pressure, p_m are used to for determining the contact reaction forces. The amount of indent depends on the angle of the taper, how far the ball has moved down the taper and how hard the pipe material is in comparison to the hardness of the ball. Typically, the ball is 2-3 times harder than the

pipe material and twice as hard as the taper material (EN24T). The coefficient of rolling friction in the elastic region (when the ball indents recover elastically) can be calculated as [8]:

$$\mu_e = \alpha \left(\frac{F_v}{E'(R')^2} \right)^{1/3}, \quad (\text{eq 1})$$

where α is the fraction of energy loss and is taken as around 0.1 (10 %) [4], but can also be taken as a calculated value instead. This can be determined by taking the area under the (stress-strain) curve (AUSSC) namely; $(\sigma \varepsilon)/2$. When the ball is deforming in the elastic region, the ball tends to roll over a contact surface which behaves in a viscous manner (the amount depending on the pipe material). In theory, low and high visco-elastic values are recommended for low rolling-resistances. This is also valid for sliding balls, but as the contact area is smaller in this case, the surface deformation enters the plastic region much quicker [8]. An illustration is given in Figure 3 of how the plastic resistance comes into action. Here, A_r and r are the Hertzian contact area and radius respectively and the contact is shown in the right hand side illustration of Figure 3. H is the hardness of the contacting surface, R the radius of the ball, F_v the normal force acting on the ball and F_f the frictional force.

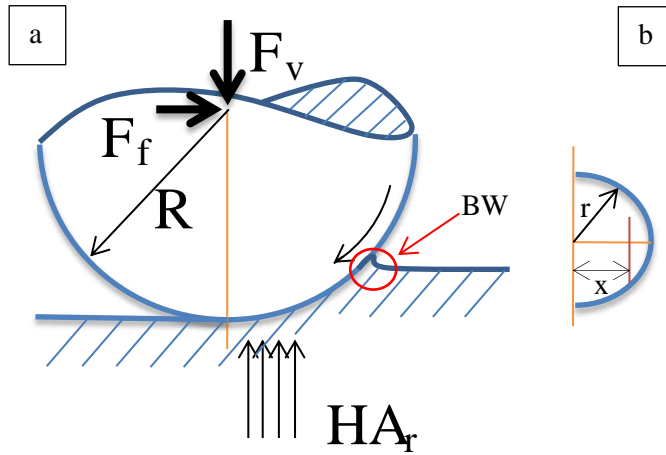


Figure 3: Plastic rolling resistance for a spherical ball, where (a) is showing the forces and ball dimension with the formation of a bow wave (BW) and b) contact area from the ball while formation of plastic indent. This is also showing the indent radius r and the distance from the centre of the ball, x .

The resistance to roll in this region starts to increase exponentially due to the plastic load and the hardness of the indenting material plays the role of contact pressure [8]. Another factor for the exponential increase in the resistance is the bow-wave which is formed in front of the moving ball. The coefficient of friction in the plastic region is given by:

$$\mu_p = 0.338 \frac{1}{R'} \sqrt{\frac{F_v}{H}}, \quad (\text{eq 2})$$

where H is the hardness [MPa] of the indented material. In this application values measured from the Brinell tests were used. There is an empirical relationship between the hardness and the (ultimate) tensile strength of a material [8, 10]:

$$H \approx \left\{ \frac{UTS}{3.5} \right\} [HBW], \quad (\text{eq 3.1})$$

or

$$H \approx 2.9 UTS [MPa] \quad (\text{eq 3.2})$$

The above equation (eq 3.1) shows that the tensile strength is a linear function of hardness with a factor of 3.5. The hardness value in the friction coefficient relationship (eq 2) is taken in terms of stress (MPa) for which eq 3.2 can be used ($HB \approx 10 \text{ MPa}$) [8, 9]. This means that a 770 HB and 550 HB corresponds to a UTS values of roughly 2.7 and 1.9 GPa for Chrome steel and the stainless steel ball respectively.

In elastic indenting, the average contact pressure is determined by dividing the normal force by the indenting area ($A_r = \pi r^2$). However, the maximum contact pressure is given as 1.5 times the average or mean contact pressure ($p_{max} = 1.5 p_m$). As the indentation steps into the yield region, it enters the elastic-plastic region with properties of elasticity and plasticity. Here, the contact pressure distribution differs from that of the elastic one and the average contact pressure is given by:

$$p_m = 0.153 \left\{ P_H \left(E' / R' \right)^2 \right\}^{1/3} \quad (\text{eq 4})$$

where P_H is the normal force which is responsible for the deformations in the elastic-plastic region and is usually lower than the critical or Hertzian load, P_c (load where the material goes beyond yield). P_c can be calculated using following expression [8]:

$$\frac{p_m}{p_{mc}} = \left(\frac{F_v}{P_c} \right)^{1/3}, \quad (\text{eq 5})$$

where p_{mc} is the yield strength of the material. Note that if $p_m = p_{mc}$, P (or P_H) = P_c which corresponds to material being deformed at the Hertzian load (the point from where deformation is not elastic anymore.)

2.3. Transition from roll to skid

There are '*potential*' features which lead to transition to a skid from rolling and are discussed next. During successful indentation, the ball tends to roll from the start to finish of the activation(s). Normally, it is believed that a successful indent relates to a pure rolling movement, but that is not true as there is some skid element present at all times, be it aligned with the normal force or either side of the ball to the contact surface. The region close to normal to the ball is associated with the roll while the region away with the slip or skid. Due to this phenomenon described as Reynolds slip, there is never pure rolling in real terms; Reynolds slip is always present as shown in Figure 4 [8, 11].

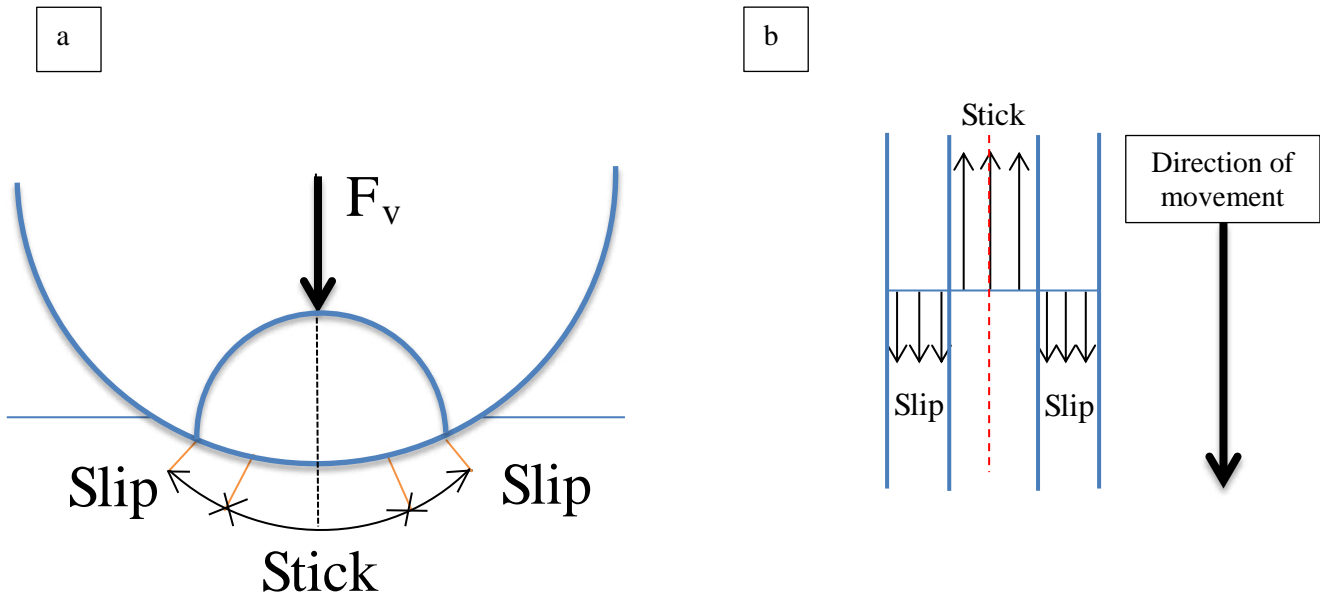


Figure 4: Front a) and top b) view of a Reynolds slip, central stick zone and illustration of resulting forces from slip and stick zones.

Another aspect of the indent phenomenon is that when the ball starts indenting in the plastic region, the resistance to roll increases substantially and exponentially as a result of trying to cope with the bow wave and indenting plastically. Increasing load applied in this region will result in an exponential increase in the resistance to roll further.

According to theory, the transition from roll to skid and combinations of these is affected by [7, 10, 11]: 1) normal force, 2) axial force, 3) ball size, 4) effective elastic modulus, 5) Poisson's ratio, 6) hardness and 7) contact friction coefficients.

The ball, while moving can switch between rolling and sliding and may do many times. This means that in reality, at a given point, a ball does not have a pure rolling element and a sliding ball can be purely skidding without any rolling element. If the balls starts off skidding very early (axial force higher than the frictional force), it tends to keep on sliding until the very end of the activation process unless the material properties, such as hardness, or friction change significantly. This is because if the traction and other resistive forces become larger, but more suitable for rolling (rolling resistance is lower), the ball can start rolling again. On

the other hand, if the ball keeps rolling, but the plastic resistance keeps increasing to the point that it exceeds the rolling force (ball rolls down the taper to the left in Figure 1b) it enters a skidding or sliding motion and the resistance from the plastic indent and bow wave (Figure 3) increases exponentially. According to equation 1, the ball size and the effective Young's modulus should be large to have a low rolling resistance. Similarly for equation 2, large ball size is more preferable. An optimal ball size can be achieved by analysing the criteria of equation 5 for each ball size and considering a factor of safety. In the yield zone and beyond, the ball indents according to the criterion given in equation 5.

The plastic resistance grows exponentially with every amount of indent in the region. So in essence, the ball can slide due to low effective Elastic modulus (elastic region), small ball size (elastic/plastic region), large vertical and axial load and high hardness value of the indenting material.

2.4. Contact stress of balls on pipe surface (a Hertzian problem)

Once the taper houses are activated, the balls start to move. When the balls roll, they indent into the material and are responsible for causing contact stresses. The pressure distribution at the point of contact is given as follows [8, 11, 12, 17, 18, 19]:

$$p(a) = -p_{max}\sqrt{(1 - a^2)}, \quad (\text{eq 6})$$

where a is the normalised contact radius $(x/r)^2$ and p_{max} is the maximum contact pressure. For calculating the radial and normal stresses, the contact pressure is integrated with respect to contact radius to give results as follows [12]:

$$\frac{\sigma_{\theta\theta}}{-p_{max}} = \frac{1-2\nu}{3} \frac{1}{a^2} \left[1 - \left(\frac{z}{\sqrt{u}} \right)^3 \right] + \frac{z}{\sqrt{u}} \left[2\nu + \frac{(1-\nu)u}{1+u} - (1+\nu)\sqrt{u} \tan^{-1} \left(\frac{1}{\sqrt{u}} \right) \right], \quad (\text{eq 7})$$

where $\sigma_{\theta\theta}$ is the radial stress, z is the material depth, and ν is the poison's ratio of the indenting material.

$$\frac{\sigma_{zz}}{-p_{max}} = \left(\frac{z}{\sqrt{u}} \right)^3 \frac{u}{u^2+z^2}, \quad (\text{eq 8})$$

where σ_{zz} is the normal stress in the z direction and u is given by:

$$u^2 = \frac{1}{2} \left\{ a^2 + z^2 - 1 + \sqrt{[(a^2 + z^2 - 1)^2 + 4z^2]} \right\}. \quad (\text{eq 9})$$

When the sphere or ball is sliding, the problem can be considered in Cartesian coordinates given that the problem is not axi-symmetric any more. From this point $g(b)$ (Appendix A) can be substituted which is used to get the stress components and displacements with superscript N (due to normal load) and T (due to traction or tangential load, μ is the coefficient of traction). The stress in the x direction, σ_{xx}^N , and the shear-stress in the $x - y$ direction, τ_{xy}^N , z direction, σ_{zz}^N , $x - z$ direction, τ_{xz}^N and $y - z$ direction, τ_{yz}^N due to normal load are also provided in the Appendix. The stresses due to traction in the x direction, σ_{xx}^T , y direction, σ_{yy}^T , z direction, σ_{zz}^T , $y - z$ direction, τ_{yz}^T , $z - x$ direction, τ_{zx}^T , $x - y$ direction, τ_{xy}^T are similarly given in Appendix A.

The total stress in any direction, will be the sum of stresses in that direction due to normal and traction forces. This leads to the maximum shear stress (with traction) evaluated as follows [11]:

$$\tau_{max} = \frac{1}{2} \sqrt{ \{ (\sigma_{xx}^S) - (\sigma_{zz}^S) \}^2 + 4 (\tau_{xz}^S)^2 } \quad | \quad (\text{eq 10})$$

where superscript *S* indicates the sum of stresses in the respective directions.

2.5. Maximum shear stress locations from the analytical model

The traction of the ball relates to the amount of traction coefficient in action or how much the ball slides. The traction coefficient can be measured from the amount of sliding during the ball indent process. If the ball is purely rolling (theoretically), the traction coefficient is zero (traction coefficient is different from rolling coefficient). Once the ball starts to slide with some rolling or the slide to roll ratio has increased, the traction coefficient starts coming into play. Figure 5 shows the changes in subsurface stress as motion changes. The arrow pointing to the right indicates direction of horizontal motion and the other arrow indicates direction of rotating motion. As this shows, the ball starts off in pure rolling wherein the maximum stress, ($\tau_{max} = 0.31 p_{max}$) is located at the centre ($x = 0$) and depth, $z = 0.48r$ (see figure 5), where r is the indent radius and p_{max} the maximum point contact stress [8, 11, 12]. Once, the ball starts sliding (due to change in surface conditions or loading etc.), the traction force pushes the maximum shear stress location slightly towards the rolling/sliding direction and away from the centre. As the traction force increases, the maximum shear-stress location moves away from the centre and towards the rolling/sliding direction. However, at a traction coefficient of 0.3, the locality of the maximum shear stress starts forming behind the ball rolling/sliding direction [8, 9]. So in essence, the shear stress distributions depict the amount of roll or skid element during ball activation.

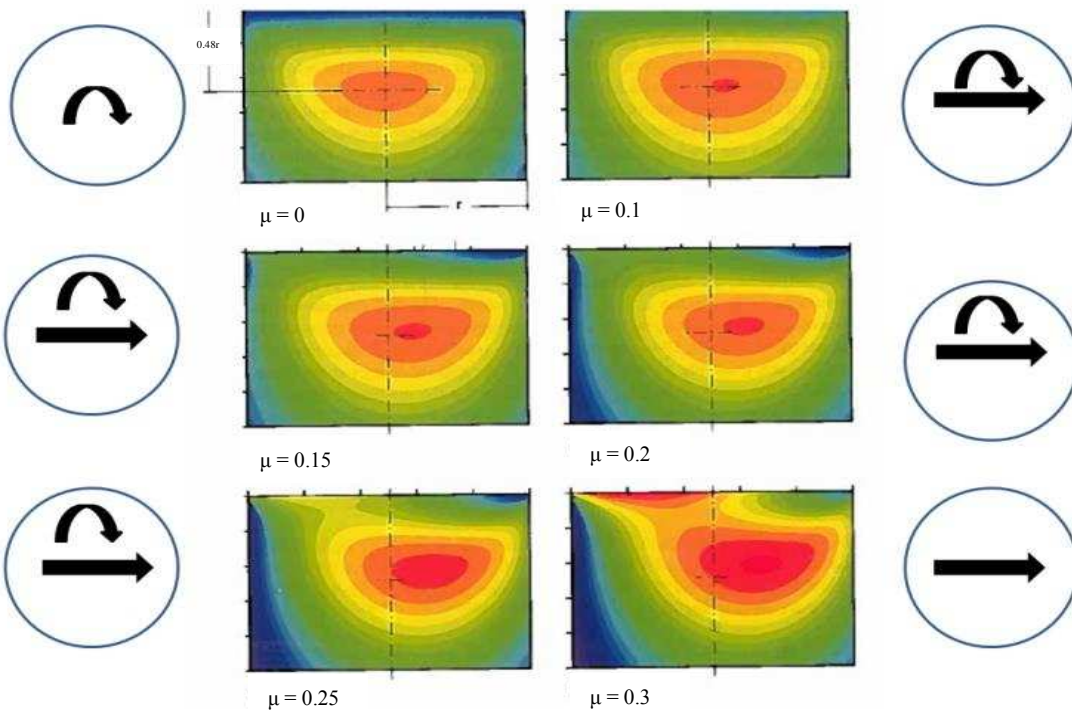


Figure 5: Illustration of Maximum shear stress contour showing distribution subject to change in traction coefficient as consequence of sliding element of steel ball for $v=0.3$ [8,11, 12].

In general, it is assumed that the surface finish is homogeneous and that the traction forces are constant. In reality any surface finish will vary and the traction forces change accordingly. In terms of amount of an indent, the contour plots in Figure 5 do not depict the amount of shear-stress and if it is in an elastic/ elastic-plastic or plastic zone. The red or dark orange zone is the area of maximum shear stress and that zone increases with the amount of indent radius which corresponds to amount of total elastic/plastic indent. In Figure 1b, the ball sits in the left part of the taper housing and starts rolling and most of the deformations are in the elastic region. As the ball moves down the taper, the ball starts to indent more but because the material has entered the plastic zone, the surface starts to collapse and progresses (unrecovered) towards a teardrop formation.

2.6. Successful and unsuccessful indent profiles

The analytical model discussed in the previous section can be used to explain the reason why the ball skidding does not form a teardrop on the surface of the pipe. During skidding, the maximum shear stress location is close or on the surface (depending on the traction coefficient). The surface below this location (subsurface) still remain elastic and the surface undergoes high stress (beyond yield) which leads the surface to form a scar (or groove). Opposed to this phenomenon, during rolling, the area near the surface remains still elastic and the maximum shear stress is located subsurface. As the ball rolls further with a higher radial force, the maximum shear stress area/volume increases subsurface where the region collapses and facilitates a tear drop formation as shown in Figure 6.

Once the subsurface stress and their locations can be predicted based on an analytical model built using stress equations of the previous section, the contour plot of the distribution of yield is reached). As seen, the maximum shear value remains subsurface and indicates pure rolling in theory. During unsuccessful indent(s), the maximum shear stress starts relocating itself away from the subsurface centre and towards the surface in the direction of ball movement (illustrated in Figure 7). The location and values are correlated with the amount of traction coefficient during the movement. The higher the traction coefficient, the more the ball skids, and the more the maximum shear stress starts relocating towards the surface. The highest maximum shear stress value can be retained subsurface if the traction coefficient is equal to or lower than 0.3. With a value of 0.5 (corresponding to rough surfaces), the maximum shear-stress is located at the surface behind the ball movement (instead of in front of it) [7, 8, 13-16].

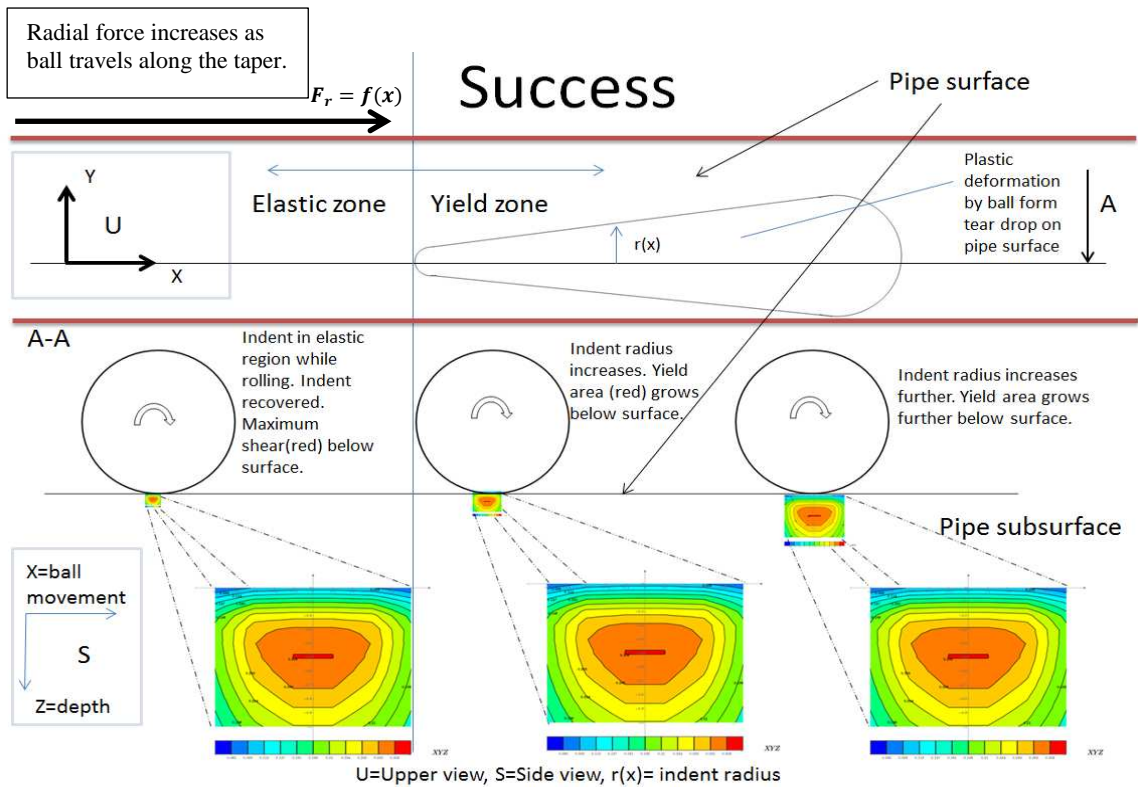


Figure 6: Successful indentation profile vs subsurface shear stress distribution.

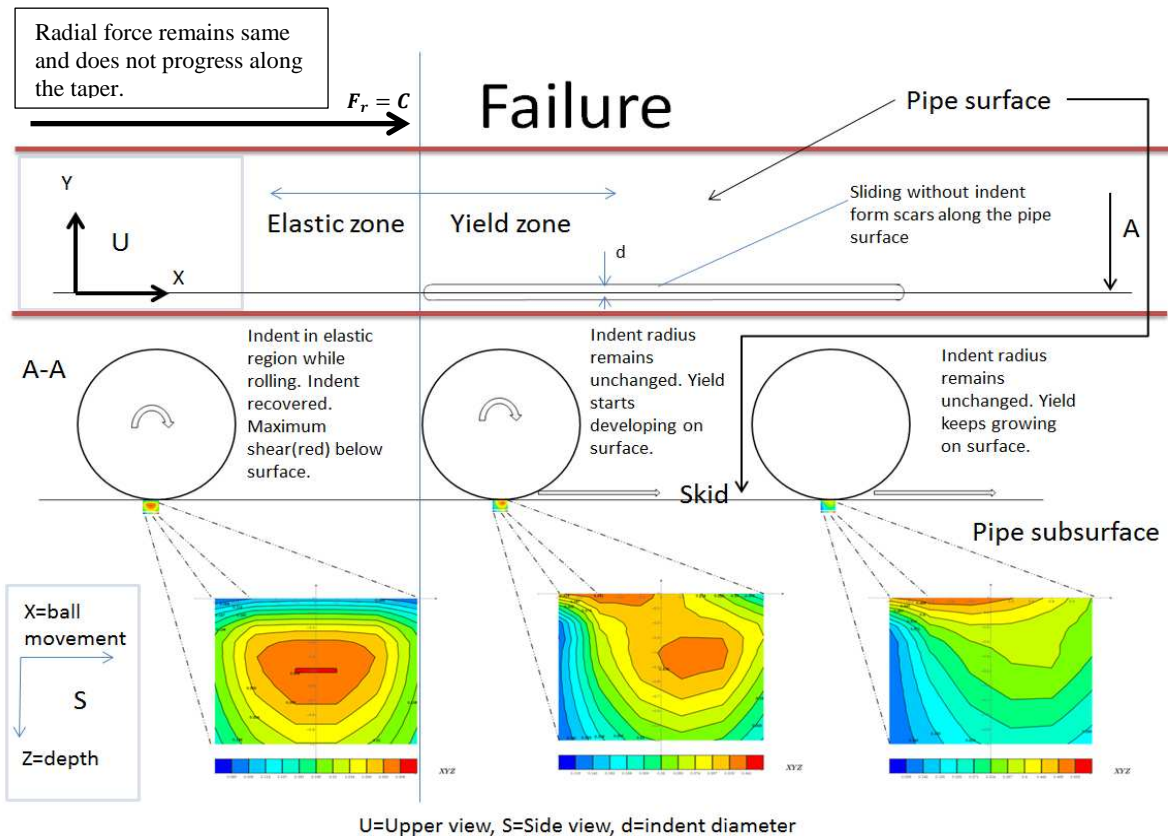


Figure 7: Unsuccessful indentation profile vs (sub) surface shear stress distribution.

If the maximum stress value is located at the surface the ball can essentially glide on the surface as the contact surface has reached 'near' yield value and in the vicinity of maximum stress.

The pipe surface has become viscous in this region. In this region, the radial or the normal force on the ball does not increase as the ball does not roll down the taper and gets pinched between the taper and pipe surfaces. This leads to visual scratches from plastic deformation on the pipe surface with a minute ball contact area.

3. EXPERIMENTAL DETAILS

Tribological experiments were planned to validate the models and to investigate features which could lead to or assist in the skidding of the ball. The approach was as follows:

- Perform mechanical tests which can replicate the activation on a small scale
- Analyse the friction and reaction forces during the tests
- Analyse the top and sub-surface of specimen that underwent permanent deformations
- Compare results with the analytical model

3.1. Specimens

There were specific materials to choose from considering the current pipe and taper house materials used as part of the mechanical connector products design. The pipe material ranges from low to high carbon steels. For the tests the materials used were EN3B (low carbon steel), 17/4 PH (stainless steel) and EN24T (high carbon steel). Please note that EN24T was used for the taper house material because of its high strength. The hardness and tensile strength values for the materials are given in Table 1. A Bruker ® UMT 3 tribometer as shown in Figure 8 was used for the experiments on the materials.

The machine allows the ball to be placed inside a ball-holder which is then pushed onto the test specimen. This specimen is fixed on a plate which is moved linearly with an electric motor. The controls of the machine are configured before the start of the procedures. A tribometer schematic is shown in Figure 8. In the schematic, the ball sits in the ball holder which remains static while the ball is free to roll. Gradually an increasing vertical forces is applied on the ball holder which then transferred onto the ball and this finally exerts force onto the indenting material. The indenting material is clamped in a specifically designed sample holder and is fixed on a plate which can travel either forward or backwards (using an electric motor) with a speed V_x (~0.15 mm/s). These fixtures ensure that the ball (5 & 6 mm; EN31) can move along the material axially by exerting a normal force (0 – 65kgf) at the same time in a controlled fashion. The ball was kept static for the initial 20 seconds (0 – 10kgf) and then allowed to move with increasing normal load up to 65kgf. The machine provides reaction forces in the three directions (plane of horizontal plate and horizontal axes), coefficient of friction, and speed of the ball holder and how far the bottom plate has moved for dry conditions. The configurations of the controls are such that they replicate the ball-indent mechanism of ball

onto a flat surface. The experiments were performed to have a scar length of at least 3 times the size of the diameter of the ball. Table 1 shows the predictions of maximum shear stress wherein tested (in their elastic limits) values of elastic modulus and Poisson's ratios are given as well. Please note that the maximum shear stress prediction does not depend on the hardness or UTS of a material. However, if the material has been deformed plastically and hardness or UTS values are known, the relative friction coefficient can be predicted.

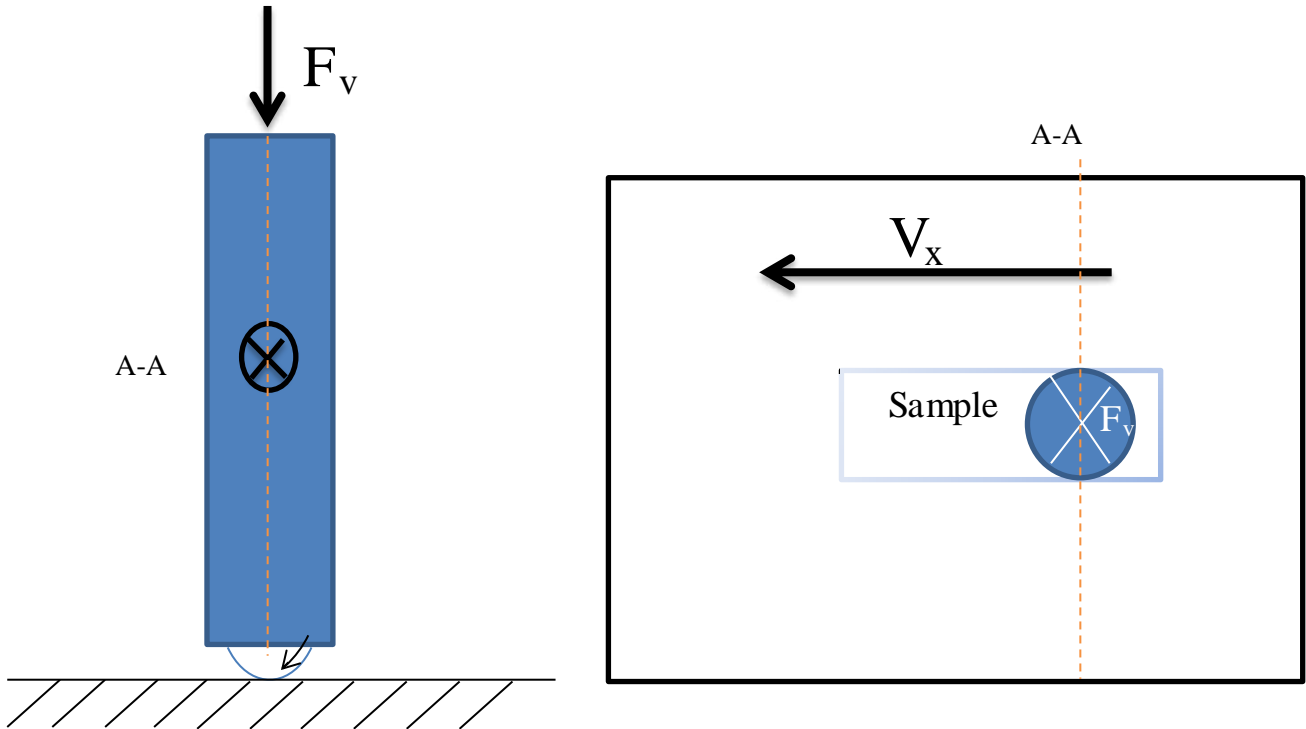


Figure 8: Schematic of the tribometer test procedure. Ball holder is static with increasing loads F_v on the ball, while the plate (with the sample) moves with a speed of V_x . Sample is fixed with a clamp onto the plate.

Finally some microscopic analysis was done to measure small profile features and compare indent subsurface microstructures.

Table 1: Predicted values of the Maximum shear stress factor for different materials based on maximum traction coefficient of 0.15. Tested values of ν and E have been provided. The UTS and H for these materials are also given.

Material	Tested ν	Tested E (GPa)	Hardness H (HBW)	UTS (MPa)	Predicted τ_{max} / P_{max}
EN3B	0.3	196.9	179	620	0.313
EN24T	0.22	207.2	283	900	0.331
17-4 PH	0.29	203.9	277	980	0.315

4. RESULTS

Figure 10 shows the variation in coefficient of rolling/traction during the ball movement over the indenting material. The normal force (ball being pressed onto material) keeps on increasing gradually regardless of the ball being moved axially or not. During the initial 20 seconds, the ball is kept still while the forces increase to get a firm grip with the material. The sample is then allowed to move with respect to the ball while the forces gradually increase, it is in this region we would like to observe any rolling/skidding element of the

ball while trying to indent into the material. As shown at around 20-23 seconds, the ball has reached its peak of static friction coefficient and beyond this the ball will be either rolling or skidding.

Depending on whether the ball has already reached plastic deformation before any forward movement, it should give an indication of the amount of resistance it has to cope with. A fully plastic indent gives higher resistance compared to attempts to indent in the elastic region. In Figure 9, the region between 23 and 56 seconds seems to have a steeper slope compared to the rest. The (thin) red lines are drawn for the mean of the graph for the particular regions. In the region between 56 and 69 seconds, the mean seems to be flattened out (~ 0 slope). The rest of the graph has fairly stable growth with a low slope. From the theory we know as the ball rolls into the plastic region, the ball is receiving high rolling resistance from the hardness of the material and bow-wave formation ahead. If the resistive force tips over the rolling moment force, the ball has to follow the traction forces in the direction of the ball movement. If the vertical force exerted remains the same, the ball will remain in its skidding motion considering the material surface is uniform throughout the movement of the ball. In this case, the forces keep increasing and there is no way of predicting beforehand the point of tipping over so that the force can be kept constant to see its effect. And as the force increases, the ball deformation at the contact phase increases at the same time which also contributes in the increase in the frictional forces both ways (rolling and sliding).

In Figure 10, it can be seen that the slopes for 17/4 PH do not flatten-out, but the initial part (26-54 seconds) has a steeper slope based on the mean for this region. The vertical force increases, and the resistive forces (opposite to the ball movement) also increase, but less steepness could indicate the ball being in a sliding motion. The same kind of behaviour for material EN24T (taper house material) can be seen in Figure 11. This does not have a zero slope and one initial section has a steeper slope than the rest. However, it can be seen that the stainless steel (17/4 PH) has a more steep slope ($\mu = 0.117 - 0.14$) compared to the taper material ($\mu = 0.122 - 0.136$) which suggests that there was more frictional resistance for the 17/4 PH material. Whether the ball has a greater rolling element in this region cannot be concluded from these graphs, how far the ball has indented has to be measured instead. The higher friction could be a consequence of the ball deforming at the same time the ball tries to indent into the material, and higher indenting material strength contributes to more ball deformation. The more the ball deforms, the larger the contact area becomes and the more the friction increases. In order to see if the increase in friction is from the increase in ball deformation or larger indent, an indent measurement needs to be done effectively. The amount of indentation indicates the amount of rolling versus sliding element, wherein theoretically rolling contributes to large indent depth compared to surface sliding. In the initial phase of the experiments, the ball has a lower normal force which means it has to roll enough in order to keep indenting further. In the later phase (towards the end), the normal force is large enough to keep the ball indenting regardless of the ball sliding or rolling. The main difference with the actual application is that the normal force is limited to the position of the ball in the taper housing (Figure 1b), whereas in the experiments, the normal force is gradually increased.

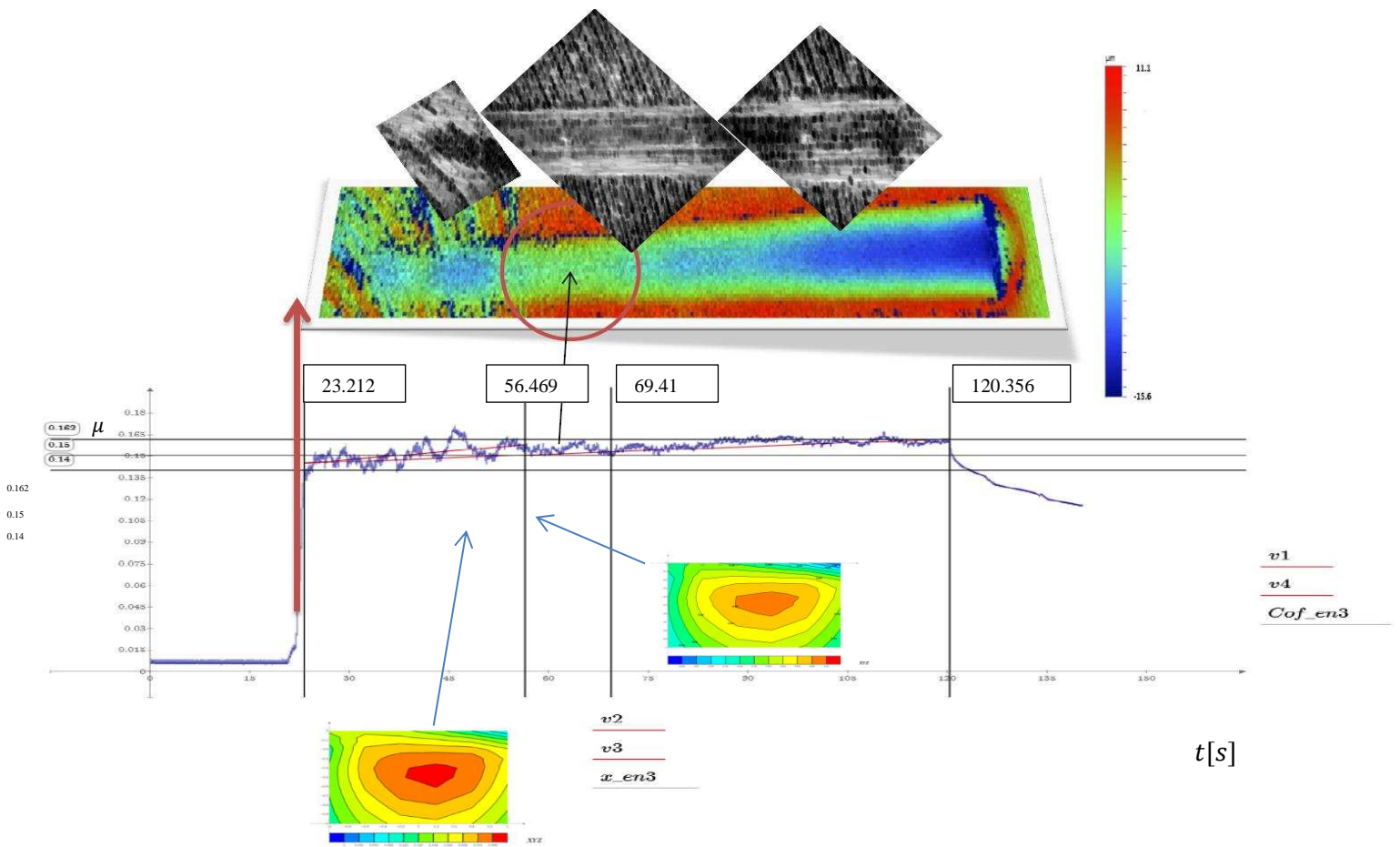


Figure 9: Coherence between friction coefficients, indent depths, extrusion marks, and shear stress for EN3B.

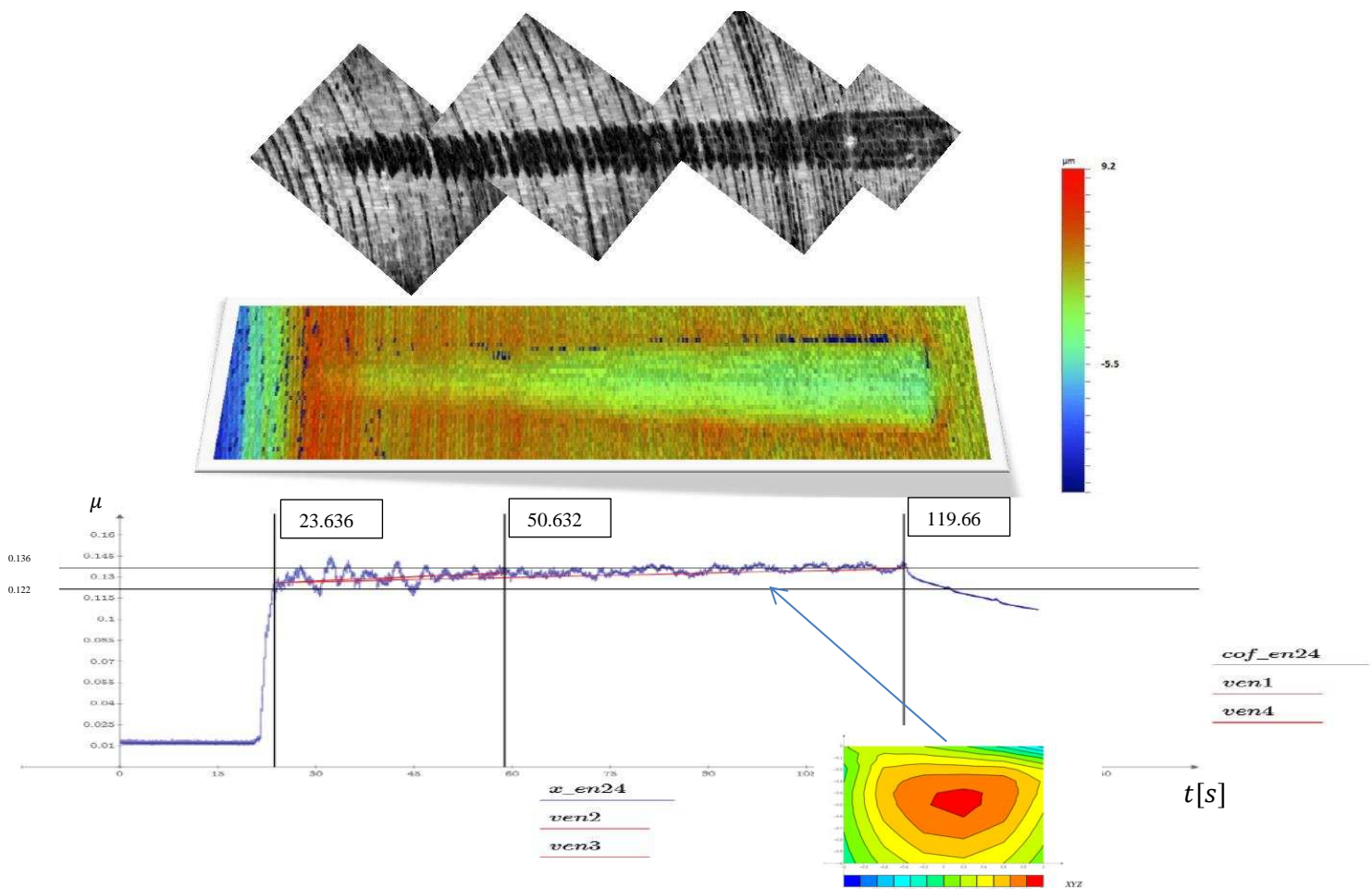


Figure 10: Coherence between friction coefficients, indent depths, extrusion marks, and shear stress for EN24T.

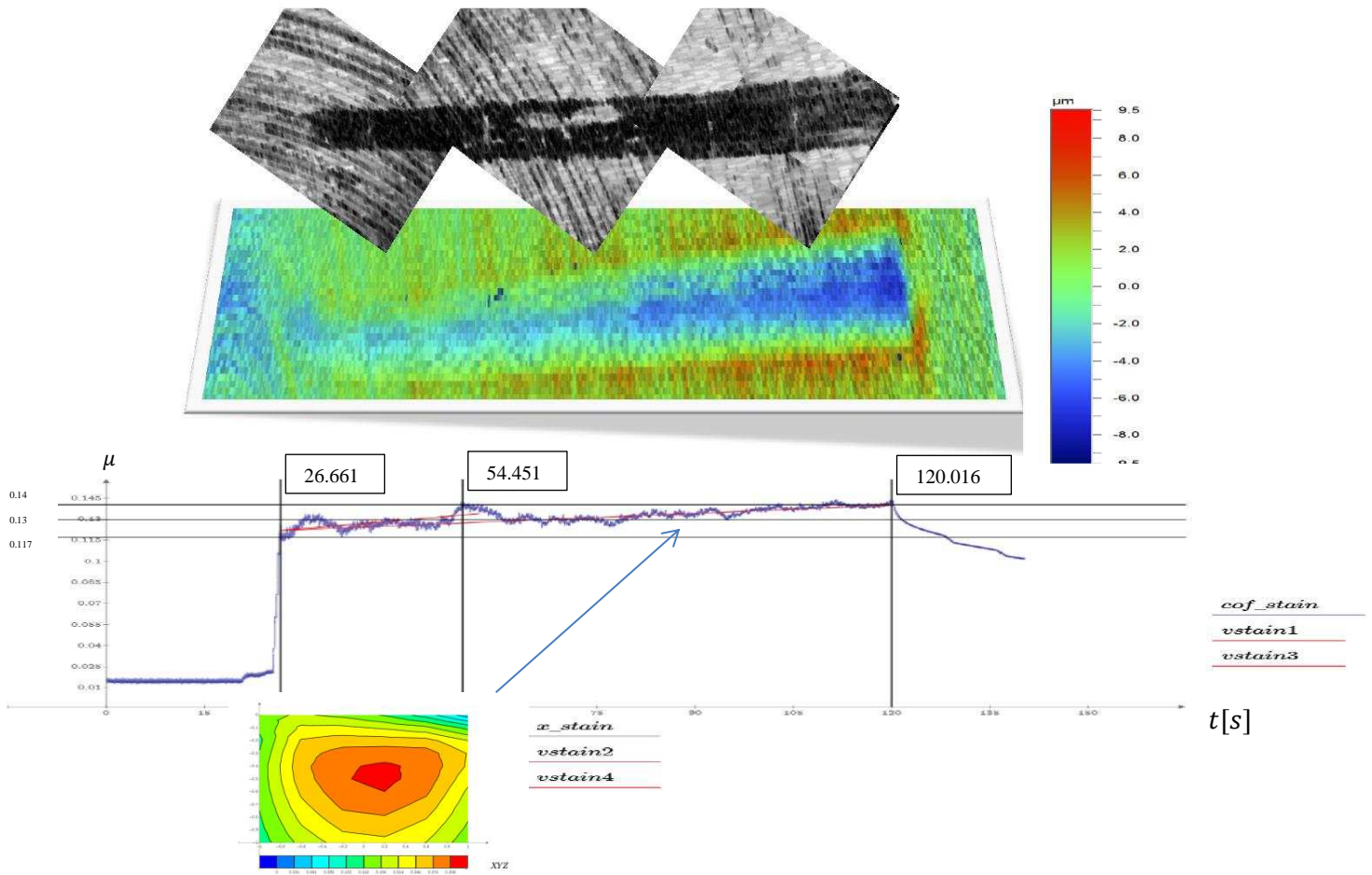


Figure 11: Coherence between friction coefficients, indent depths, extrusion marks, and shear stress for 17/4 PH.

5. Discussion

Finally, to see if there is any coherence between them, the different results must be put together. The friction coefficient graph, indent depth contour map and the extrusion marks are overlaid. For Figure 9, the circled location correlates with the friction coefficient graph going flat. Also, in the extrusion images, there are clear extrusion marks which indicate the material had a high skidding element. There will always be some extrusion marks along the two sides as these are considered as the stick zone for the ball. Moreover, the analytical model showed the ball is skidding using the inputs from the friction graph and material properties.

When the ball skids, the location of the maximum shear stress is no longer near the centre of the moving ball, but has shifted towards the surface. The more the maximum shear stress location gets pushed towards the surface, but it is still close to the centre of the moving ball (average μ at region of flattening is $0.15 < 0.3$). Here, the principle maximum shear stress, $\tau_{max} = 0.378 p_{max}$ at a depth of $0.45r$ (z) and $0.17r$ (x) from the centre of the ball. For Figures 10 and 11, there is clear correlation between the friction graphs (clear steep slopes) and the indent profiles (no long light patches in length of the scar). $\tau_{max} = 0.31 p_{max}$ for 17/PH ($0.48r$ (z) depth and $0.11r$ (x) from centre) and $0.31 p_{max}$ for EN24T ($0.48r$ (z) depth and $0.12r$ (x) from centre).

For 17/4 PH though there is a small patch of extrusion mark which relates to the indent graph (light area in the location) and some local flattening in the graph. However, this could relate to a surface imperfection as there are no any irregularities before and after this location. This patch is certainly less severe as compared to EN3B. Softer material has higher tendency to indent more compared to hard materials so it can be concluded that this can be related to the surface condition not being homogenous and given the fact the ball is small (5mm) for this experiment, a small change can lead to the ball not being able to indent properly with deformation along its path. The larger the deformation of the ball, the larger surface area is in contact, and the more frictional resistance plays roll in forcing it to skid.

Frictional experimentation on the tribometer showed changes in the friction coefficients while the precision ball was allowed to move axially on a flat plate by gradually increasing the pressure on the ball. This procedure replicates the behaviour of the ball during the connector activation. Once the ball is free to move, the friction coefficient rises, flattens and dips (considering a moving average). The rising would indicate a high rolling element of the ball, flattening as a high sliding element and dipping as structural collapse at the end with pure sliding. For the plastic indentations, rolling friction is always higher than the sliding friction $\mu_p \propto (F_v/H)^{1/2}$ ($\mu_e \propto (F_v/E)^{1/3}$). The large increase in plastic rolling friction pushes the ball to transition into sliding. In pure terms, there is always a sliding element as a consequence of a constant presence of a stick zone. The transition from rolling to pure sliding happens once the rolling frictional resistances and traction forces overcome the rolling forces and tractional friction.

The images from the optical microscopy show the indentation and extrusion marks for the indent profiles. The extrusion marks from the sides of the indent profiles were as expected. They clearly show aforementioned stick-zone. Any extrusion marks away from the stick zone could mean ball is in the sliding mode.

Overall, the analytical model fits well the experimental data since the friction values from the experiments provided the maximum shear stress locations. Combining all the test results together it appeared there was a close coherence between them location wise. When the friction graph flattens, there are clear extrusion marks at the same spot. Also the profile depth is minimum (from the profilometer results) at this region. Moreover, the shear-stress contour plot from the analytical model suggests sliding for the same region. Because of the fact that the tests were performed at a smaller scale, and the smaller surface changes (sudden roughness change) can lead to ball not being able to indent properly, and adding the amount of deformation at the force increment, the ball can transition from roll to skid more quickly. The analytical model fits well with the experiments conducted. When the ball appears to be sliding or rolling, depending on the amount of traction, the maximum shear stress location (indicator of slide/roll elements) is moving towards the surface. If the ball is purely sliding, this location shifts towards the surface even more. The model helps to back up the amount of sliding by evaluating the amount of shear stress and the locations with respect to the top surface.

6. CONCLUSIONS

The integrity of the mechanical connector product is focused on a strong mechanical grip between pipes. The latter is achieved by precision steel balls placed circumferentially around the connector. After having discussed the background and test procedures and results, the following can be concluded:

- The precision ball indentation procedure was analysed to detect features leading to slide/skids. According to theory, a rolling sphere transitions from rolling into skidding due to significant differences in the coefficient of friction between the different contact surfaces, the amount of normal and axial forces, the effective (based on shape of contacting bodies) elastic modulus, hardness of indenting material and lastly, but not the least, the size of the ball.
- The analytical model gives an insight to the amount of skidding based on the friction values and certain material properties such as Poisson's ratio and Young's Modulus for the bodies in contact. When the maximum shear stress location moves towards the surface, it indicates the ball is in a sliding mode, but when it is more centred around a certain depth, the ball is in a rolling mode. The point of maximum shear grows as the amount of pressure increases and when the maximum shear enters the plastic zone, there is a permanent deformation (collapse of subsurface material) due to which the ball makes a permanent deformation. The models are validated once input parameters are known from the experiments.
- The analytical model will be a subject to continuous improvement under similar test conditions which will also cover other contact types such as elliptical. The elliptical contact model can be used for analysing the indent of the ball on the taper housing which is also known as back-indent.

- To improve confidence of the models, experiments will be performed in a scaled-up version of the tests discussed in the paper.

7. ACKNOWLEDGEMENTS

The authors would like to thank the funding body, Innovate UK (KTP009526) and especially Hydratight UK for both its financial and technical support for this project.

8. REFERENCES

- [1] B. Hall, "Prevention of ball skidding in connectors. " Design report, (2012).
- [2] D. N. Olaru, and C. Stamate, and A. Dumitrascu, and G. Prisacaru, "New micro tribometer for rolling friction." *Wear* 271.5 (2011): 842-852.
- [3] M. R. Balan, and D. Olaru. "Rolling friction torque in lubricated contacts from micro to macro scale." *Mechanical Testing and Diagnosis*, 2 (2012): 44-53.
- [4] G. Taylor. "Design of mechanical pipe coupling. " Hydratight design procedures, (2005).
- [5] G. M. Pharr, and W. C. Oliver, and F. R. Brotzen. "On the generality of the relationship among contact stiffness, contact area, and elastic modulus during indentation." *Journal of materials research* 7.03 (1992): 613-617.
- [6] W. C. Oliver, and G. M. Pharr. "An improved technique for determining hardness and elastic modulus using load and displacement sensing indentation experiments." *Journal of materials research* 7.06 (1992): 1564-1583.
- [7] J. Archard, "Contact and rubbing of flat surfaces." *Journal of applied physics* 24.8 (1953): 981-988.
- [8] A. van Beek, "Advanced engineering design." TU Delft, (2006).
- [9] L. Ma, and S. Low, and J. Song. "Investigation of Brinell indentation diameter from confocal microscope measurement and FEA modeling." *Proceedings of Hardmeko* (2007): 19-21.
- [10] W.D. Callister, and D.G. Rethwisch. "Materials science and engineering: an introduction. " New York: Wiley, (2007).
- [11] K. L. Johnson, "Contact mechanics. " Cambridge University Press, (1987).
- [12] D. A. Hills, and D. Nowell, and A. Sackfield. "Mechanics of elastic contacts." BH ltd (1993).
- [13] E. R. Kral, and K. Komvopoulos. "Three-dimensional finite element analysis of subsurface stress and strain fields due to sliding contact on an elastic-plastic layered medium." *Journal of tribology* 119.2 (1997): 332-341.
- [14] J. E. Merwin, and K. L. Johnson. "An analysis of plastic deformation in rolling contact." *Proceedings of the Institution of Mechanical Engineers* 177.1 (1963): 676-690.
- [15] D. M. Bailey, and R. S. Sayles. "Effect of roughness and sliding friction on contact stresses." *Journal of tribology* 113.4 (1991): 729-738.
- [16] K. L. Johnson, "The strength of surfaces in rolling contact." *Proceedings of the Institution of Mechanical Engineers, Part C: Journal of Mechanical Engineering Science* 203.3 (1989): 151-163.
- [17] S. P. Timoshenko, and J. N. Goodier. "Theory of Elasticity." NY, McGraw Hill, (1951).

- [18] S. P. Timoshenko, and J. N. Goodier. "Theory of Elasticity." NY, McGraw Hill, 2nd ed., (1970).
- [19] S. P. Timoshenko, and J. N. Goodier. "Theory of Elasticity." NY, McGraw Hill, 3rd ed., (1982).
- [20] M. Kaneta, and T. Sakai, and H. Nishikawa. "Effects of surface roughness on point contact EHL." Tribology Transactions 36.4 (1993): 605-612.
- [21] L. Kogut, and I. Etsion. "A static friction model for elastic-plastic contacting rough surfaces." Transactions of the ASME-F-Journal of Tribology 126.1 (2004): 34-40.
- [22] B. Bhushan. "Contact mechanics of rough surfaces in tribology: multiple asperity contact." Tribology letters 4.1 (1998): 1-35.
- [23] D. Bogy, and R. Kaneko. "Nanoindentation hardness tests using a point contact microscope." Journal of tribology 116 (1994): 175.

APPENDIX A

(Expressions for analytical model from Hills et al. (1993) [12])

$$\frac{\sigma_{\theta\theta}}{-p_{max}} = \frac{1-2\nu}{3} \frac{1}{a^2} \left[1 - \left(\frac{z}{\sqrt{u}} \right)^3 \right] + \frac{z}{\sqrt{u}} \left[2\nu + \frac{(1-\nu)u}{1+u} - (1+\nu) \sqrt{u} \tan^{-1} \left(\frac{1}{\sqrt{u}} \right) \right],$$

where $\sigma_{\theta\theta}$ is the radial stress, z is the material depth, ν is the poisson's ratio of the indenting material.

$$\frac{\sigma_{zz}}{-p_{max}} = \left(\frac{z}{\sqrt{u}} \right)^3 \frac{u}{u^2+z^2},$$

where σ_{zz} is the normal stress in the z direction and u is given by:

$$u^2 = \frac{1}{2} \left\{ a^2 + z^2 - 1 + \sqrt{[(a^2 + z^2 - 1)^2 + 4z^2]} \right\}.$$

On the $a = 0$ axis, the relations are as follows:

$$\frac{\sigma_{\theta\theta}}{-p_{max}} = (1+\nu) \left[1 - z \tan^{-1} \left(\frac{1}{z} \right) \right] - \frac{1}{2(1+z^2)}.$$

$$\frac{\sigma_{zz}}{-p_{max}} = \frac{1}{1+z^2},$$

$$\tau_{z\theta} = 0.$$

On the surface within the contact patch the relations are as follows:

$$\frac{\sigma_{\theta\theta}}{-p_{max}} = \frac{1-2\nu}{3} \frac{1}{a^2} \left[1 - (1-r^2)^{3/2} \right] + 2\nu \sqrt{1-a^2},$$

$$\frac{\sigma_{zz}}{-p_{max}} = \sqrt{1-a^2},$$

$$\tau_{z\theta} = 0.$$

When considering the exterior of the surface to the point of contact these are:

$$\frac{\sigma_{\theta\theta}}{-p_{max}} = \frac{1-2\nu}{3} \frac{1}{a^2},$$

$$\sigma_{zz} = \tau_{z\theta} = 0.$$

Finally, at the origin these are:

$$\frac{\sigma_{zz}}{-p_{max}} = 1,$$

$$\frac{\sigma_{\theta\theta}}{-p_{max}} = \frac{1}{2} + \nu.$$

When the sphere or ball is sliding, we can consider the problem in Cartesian coordinates given that the problem isn't axi-symmetric any more. So [10]:

$$g(b) = \frac{h(b)}{\mu} = \frac{2}{\pi} \frac{d}{db} \left\{ \int_b^c \frac{ap(a)}{\sqrt{(a^2-b^2)}} da \right\} ,$$

it gives:

$$g(b) = \frac{h(b)}{\mu} = p_{max} b,$$

From this point we may substitute $g(b)$ which is used to get the stress components and displacements with superscript N (due to normal load) and T (due to traction or tangential load, μ is the coefficient of traction) as follows:

$$\frac{\sigma_{xx}^N}{p_{max}} = (1 - 2\nu) \frac{1}{3a^4} (x^2 - y^2) \left(1 - \frac{z^3}{u^3}\right) + \frac{z}{u} \left[(1 + \nu)u \tan^{-1} \left(\frac{1}{u}\right) - 2\nu - (1 - \nu) \frac{u^2}{1+u^2} - (1 - 2\nu) \frac{x^2}{a^2(1+u^2)} - \frac{x^2 u^4}{(1+u^2)^2(u^4+z^2)} \right],$$

where σ_{xx}^N is the stress in the x direction.

$$\frac{\sigma_{yy}^N}{p_{max}} = (1 - 2\nu) \frac{1}{3a^4} (x^2 - y^2) \left(\frac{z^3}{u^3} - 1\right) + \frac{z}{u} \left[(1 + \nu)u \tan^{-1} \left(\frac{1}{u}\right) - 2\nu - (1 - \nu) \frac{u^2}{1+u^2} - (1 - 2\nu) \frac{y^2}{a^2(1+u^2)} - \frac{y^2 u^4}{(1+u^2)^2(u^4+z^2)} \right],$$

where σ_{yy}^N is the stress in the y direction.

$$\frac{\tau_{xy}^N}{p_{max}} = - \frac{xyzu^3}{(1+u^2)^2(u^4+z^2)} + (1 - 2\nu)H ,$$

where τ_{xy}^N is the shear-stress in the $x - y$ direction.

$$\frac{\sigma_{zz}^N}{p_{max}} = - \frac{z^3}{u(u^4+z^2)} ,$$

where σ_{zz}^N is the stress in the z direction.

$$\frac{\tau_{xz}^N}{p_{max}} = - \frac{xz^2u}{(1+u^2)(u^4+z^2)} ,$$

where τ_{xz}^N is the shear-stress in the $x - z$ direction.

$$\frac{\tau_{yz}^N}{p_{max}} = - \frac{yz^2u}{(1+u^2)(u^4+z^2)} ,$$

where τ_{yz}^N is the shear-stress in the $y - z$ direction.

$$\frac{\sigma_{xx}^T}{\mu p_{max}} = - \left[\frac{\sigma_{yy}^T + \sigma_{zz}^T}{\mu p_m} \right] - x(1 + \nu) [\tan^{-1}(1/u) - u/(1 + u^2)] ,$$

where σ_{xx}^T is the stress in the x direction due to traction.

$$\frac{\sigma_{yy}^T}{\mu p_{max}} = 2\nu x \left[-\frac{3}{8} \tan^{-1}(1/u) + \frac{u}{4(1+u^2)^2} + \frac{3u}{8(1+u^2)} - \frac{y^2 u^5}{(1+u^2)^3(u^4+z^2)} \right] + (1 - 2\nu)z \frac{\partial H}{\partial y} ,$$

where σ_{yy}^T is the stress in the y direction due to traction.

$$\frac{\sigma_{zz}^T}{\mu p_{max}} = - \frac{xz^2u}{(1+u^2)(u^4+z^2)} ,$$

where σ_{zz}^T is the stress in the z direction due to traction.

$$\frac{\tau_{yz}^T}{\mu p_{max}} = - \frac{xyzu^3}{(1+u^2)^2(u^4+z^2)} ,$$

where τ_{yz}^T is the shear-stress in the $y - z$ direction due to traction.

$$\frac{\tau_{zx}^T}{\mu p_{max}} = z \left[\frac{3}{2} \tan^{-1}(1/u) - \frac{u}{2(1+u^2)^2} - \frac{1}{u} - \frac{x^2 u^3}{(1+u^2)^2(u^4+z^2)} \right] ,$$

where τ_{zx}^T is the shear-stress in the $z - x$ direction due to traction.

$$\frac{\tau_{xy}^T}{\mu p_{max}} = 2vy \left[\frac{1}{8} \tan^{-1}(1/u) - \frac{u}{8(1+u^2)} + \frac{u}{4(1+u^2)^2} - \frac{x^2 u^5}{(1+u^2)^3(u^4+z^2)} \right] - \frac{y}{2} \left[\tan^{-1}\left(\frac{1}{u}\right) - \frac{u}{1+u^2} \right] + (1-2v)z \frac{\partial H}{\partial x},$$

where τ_{xy}^T is the shear-stress in the $x - y$ direction due to traction.

Where:

$$a^2 = x^2 + y^2,$$

$$H = \frac{xy}{3a^4} [(z/u)^3 - 3(z/u) + 2],$$

so that:

$$\frac{\partial H}{\partial x} = H \frac{(y^2-3x^2)}{xa^2} + \frac{ux^2yz}{a^2(u^4+z^2)(1+u^2)},$$

$$\frac{\partial H}{\partial y} = H \frac{(x^2-3y^2)}{ya^2} + \frac{uxy^2z}{a^2(u^4+z^2)(1+u^2)}.$$

And u^2 is the largest root of (repeat of eq. 9):

$$\frac{a^2}{1+u^2} + \frac{z^2}{u^2} = 1$$

On the axis of symmetry ($x = y = 0$) the stress components due to normal loading are as given by:

$$\frac{\sigma_{xx}^N}{p_{max}} = \frac{1}{a^2} \left\{ \frac{y^2-x^2}{a^2} \frac{1-2v}{3} [(1-a^2)^{3/2} - 1] - (x^2 + 2vy^2) \sqrt{1-a^2} \right\},$$

$$\frac{\sigma_{yy}^N}{p_{max}} = \frac{1}{a^2} \left\{ \frac{x^2-y^2}{a^2} \frac{1-2v}{3} [(1-a^2)^{3/2} - 1] - (y^2 + 2vx^2) \sqrt{1-a^2} \right\},$$

$$\frac{\tau_{xy}^N}{-p_{max}} = (1-2v) \frac{xy}{a^2} \left\{ \sqrt{1-a^2} + \frac{2}{3a^2} [(1-a^2)^{3/2} - 1] \right\},$$

$$\tau_{yz}^N = \tau_{zx}^N = 0.$$

And outside the contact patch

$$\frac{\sigma_{xx}^N}{-p_{max}} = \frac{(1-2v)(x^2-y^2)}{3a^4},$$

$$\frac{\sigma_{yy}^N}{-p_{max}} = \frac{(1-2v)(y^2-x^2)}{3a^4},$$

$$\frac{\tau_{xy}^N}{-p_{max}} = \frac{2xy(1-2v)}{3a^4},$$

$$\tau_{yz}^N = \tau_{zx}^N = 0.$$

Turning to tangential loading, this produces only one non-zero component on the z -axis, i.e.

$$\frac{\tau_{zx}^T}{\mu p_{max}} = \frac{3}{2} z \tan^{-1}\left(\frac{1}{z}\right) - 1 - \frac{z^2}{2(1+z^2)}. \quad \text{Inside the contact patch, on the surface, the following stress}$$

components due to tangential loading are non-zero:

$$\frac{\sigma_{xx}^T}{-\mu p_{max}} = -\frac{\pi x}{2} \left(1 + \frac{v}{4}\right),$$

$$\frac{\sigma_{yy}^T}{-\mu p_{max}} = -\frac{3\pi vx}{8},$$

$$\frac{\tau_{xy}^T}{-\mu p_{max}} = \frac{\pi y}{4} \left(\frac{v}{2} - 1\right),$$

$$\frac{\tau_{zx}^T}{-\mu p_{max}} = -\sqrt{1-a^2}.$$

Lastly, on the surface outside the contact the following non-zero stress components due to tangential loading arise:

$$\frac{\sigma_{xx}^T}{-\mu p_{max}} = \frac{x}{a^4} \left\{ 2\{a^2 + vy^2\}K_0 + v \left[3 - 4 \left(\frac{x}{a} \right)^2 \right] L_0 \right\},$$

$$\frac{\sigma_{yy}^T}{-\mu p_{max}} = \frac{vx}{a^4} \left\{ 2x^2 K_0 + \left[1 - 4 \left(\frac{y}{a} \right)^2 \right] L_0 \right\},$$

$$\frac{\tau_{xy}^T}{-\mu p_{max}} = \frac{y}{a^4} \left\{ \{a^2 - 2vx^2\}K_0 + v \left[1 - 4 \left(\frac{x}{a} \right)^2 \right] L_0 \right\},$$

where:

$$K_0 = -\frac{1}{2} \sqrt{a^2 - 1} + \frac{1}{2} a^2 \tan^{-1} \left[\frac{1}{\sqrt{a^2 - 1}} \right],$$

$$L_0 = \frac{1}{2} (a^2 - 1)^{3/2} - \frac{1}{4} a^4 \tan^{-1} \left[\frac{1}{\sqrt{a^2 - 1}} \right] - \frac{1}{4} a^2 \sqrt{a^2 - 1}.$$

Hence, although the stress field associated with a sliding Hertzian axi-symmetric contact is complex, it is completely expressible in terms of elementary functions, and is easy to evaluate.